ASPECT RATIO INFLUENCE ON VORTEX STRUCTURE FORMED IN MICROCHANNELS

Cătălin Mihai BĂLAN[1], Cătălin MĂRCULESCU[1], Iulia - Rodica DAMIAN[2], Ioana - Laura OMOCEA[2]

We report here an extensive numerical investigation within a Y shape micro-bifurcation with one entry. The present study is emphasizing the influence that aspect ratio ($AR = h/w$, with $w = 700\ \mu m$ maintained constant) can have on the topology of secondary flows formed in the bifurcated area for different heights of the microchannel. In this investigation, different behaviors of the secondary flows have been distinguished within the flow domain of Reynolds number $Re \leq 100$. The vortex "movement" manifested in the closed branch of the bifurcation has been quantified in graphical representations function of Re for different AR.

Keywords*: micro-bifurcation, numerical simulations, Re -number, secondary flows*

1. Introduction

In microfluidic flows - as in classical fluid mechanics - fluids are considered continuum materials, where kinematic and dynamic quantities are continuous fields defined in the flow domain. Therefore, flow problems can be resolved by analytical solutions given by the Navier-Stokes equation along with the convection-diffusion equation. Although these solutions can be easily resolved, for the microfluidic flows, they are special: only in a few and in a highly symmetric cases it is possible to find analytical solutions [1]. Except one-dimensional configuration (channels in which the flows are manifested on parallel pathlines), numerical solutions are the only reliable procedures for the calculation of the cinematic and dynamic unknown variables in the developed application.

In CFD analyses, usually, two criteria can be identified: (*i*) validation of numerical solutions in simple configurations, where the analytical solution exists; and (*ii*) calibration of numerical solutions in complex configurations, based on experimental visualizations and measurements. Within the present application, part of the numerical results was compared with experimental investigations as benchmark problems for the validations of the numerical code (investigation conducted and presented by Balan et al. in [1]).

[1] Principal Researchers, Laboratory of Micro and Nano Fluidics L10, National Institute for R&D in Microtechnologies IMT-Bucharest, Romania, e-mail: catalin.balan@imt.ro
[2] PhD students, REOROM Laboratory, Power Engineering Faculty, University POLITEHNICA of Bucharest, Romania

The present numerical simulations of the micro hydrodynamic characterization have been performed with commercial FLUENT™ module of Ansys software. FLUENT™ is designed to solve a wide range of partial differential equations comprising most of the equations appearing in relation to fluid mechanics. All the investigated micro-fluidic flows are laminar, incompressible and take place at a relatively low Reynolds numbers ($Re < 100$).

The extensive numerical investigation was developed in a Y shape micro-geometry with one entry for different micro-channel heights, h (with an aspect ratio - AR defined as $AR = h / w$, with $w = 700\,\mu m$ maintained constant, and $h \in [70\,\mu m;\ 7000\,\mu m]$). In all numerical investigations one of the outflows was maintained closed. On these 3D geometries different behaviours of the secondary flows have been distinguished within the flow domain of $Re \leq 100$. The evolutions of the vortical structures developed in the closed branch were quantified in graphical representations as function of microchannel height and Reynolds number value.

2. Governing Equations and Numerical Method

The FLUENT™ code solves the Cauchy equation of motion in which the extra-stress tensor is expressed as a generalized Newtonian model:

$$\rho\left[\frac{\partial \boldsymbol{v}}{\partial t} + (\boldsymbol{v}\nabla)\boldsymbol{v}\right] = \rho\boldsymbol{b} - \nabla p + 2\nabla(\eta(\dot{\gamma})\boldsymbol{D}), \tag{1}$$

where ρ is the fluid density (assumed constant), $\boldsymbol{b}$ the mass force, $\boldsymbol{D}$ is the strain rate tensor, t is the time, $\boldsymbol{v}$ is the velocity vector, p is the pressure and $\eta(\dot{\gamma})$ is the viscosity function, dependent on shear rate γ. For a Newtonian fluid $\eta(\dot{\gamma}) = \eta_0$ and eq. (1) becomes the Navier-Stokes equation, as the viscous term has the simplified expression $\eta_0\Delta\boldsymbol{v}$.

The numerical code completes the equation of motion with the continuity equation which, for incompressible fluids, is reduced to $\Delta\boldsymbol{v} = 0$.

For all studied cases, the validity of fluid homogeneity and the no-slip boundary condition were assumed (see also for details [3-5]). The above governing equations are solved numerically using a finite volume method. In this methodology the resulting algebraic equations relate the dependent variables (p, $\boldsymbol{v}$) which are calculated at the center of the cells forming the computational mesh, to the values in the nearby surrounding cells. Because the interest in this work is for steady-state calculations, the time derivative is discretized with an implicit first-order Euler scheme. The physical properties of the fluids used in the numerical calculations were selected to match those of deionized water (newtonian model with $\eta_0 = 10^{-3} Pa \cdot s$).

The initial conditions imposed are: (*i*) no-slip boundary condition at the solid walls, (*ii*) uniform velocity profile and a null stress were imposed at the inlet boundary (located far upstream of the interest region) (see *Table 1*) and (*iii*) the imposed outflow boundary conditions involve vanishing stress components, respectively a constant pressure gradient (atmospheric pressure) at the channel outlet.

Table 1

The average velocities ($v_0[m \cdot s^{-1}]$) impose at the entry of the microbifurcations

Re / h $[\mu m]$	**10**	**20**	**30**	**40**	**50**	**60**	**70**	**80**	**90**	**100**
70	0.078	0.157	0.235	0.314	0.392	0.471	0.55	0.628	0.707	0.785
350	0.021	0.042	0.064	0.085	0.107	0.128	0.15	0.171	0.192	0.214
700	0.014	0.028	0.042	0.057	0.071	0.085	0.1	0.114	0.128	0.142
1400	0.011	0.021	0.032	0.042	0.053	0.064	0.075	0.085	0.096	0.107
2100	0.009	0.019	0.028	0.038	0.047	0.057	0.066	0.076	0.085	0.095
2800	0.0089	0.0178	0.0267	0.0357	0.0446	0.0535	0.0625	0.0714	0.0803	0.0892
3500	0.0085	0.0171	0.0257	0.0342	0.0428	0.0514	0.06	0.0685	0.0771	0.0857
4200	0.0083	0.0166	0.025	0.0333	0.0416	0.05	0.0583	0.0666	0.075	0.0833
4900	0.0081	0.0163	0.0244	0.0326	0.0408	0.0489	0.0571	0.0653	0.0734	0.0816
5600	0.0080	0.0160	0.0241	0.0321	0.0401	0.0482	0.0562	0.0642	0.0723	0.0803
6300	0.0079	0.0158	0.0238	0.0317	0.0396	0.0476	0.0555	0.0634	0.0714	0.0793
7000	0.0078	0.0157	0.0235	0.0314	0.0392	0.0471	0.055	0.0628	0.0707	0.0785

3. Computational Domain, Meshes and Dimensionless Numbers

Table 2 provides an enlarged view of typical meshes used in the numerical computations near the bifurcation area. The length of the bifurcation branches are set to be longer than in the actual experimental devices to ensure that the flows fully develop upstream of the bifurcations and completely re-develop downstream on the open branches. Block-structured orthogonal meshes are used to map the computational domains. The computational meshes have a total number of cells (NC) varying from 192.000 to $2.880.000$. The most important geometric parameter considered for this application is the aspect ratio (AR), defined as $AR = h/w$, which varies from 0.1 to 10.

Table 2

The influence of aspect ratio *AR* over the domain discretization parameters

h [μm]	View of the mesh with a detail near the bifurcation	Number of cells	h [μm]	View of the mesh with a detail near the bifurcation	Number of cells
70	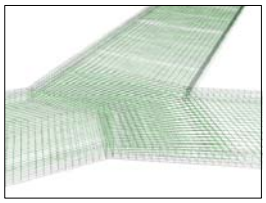	192.000	**3500**	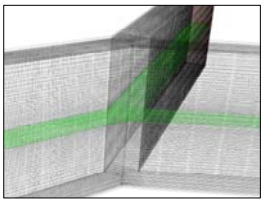	1.680.000
350	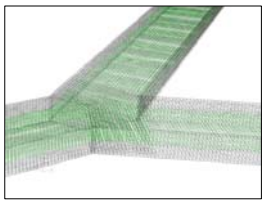	384.000	**4200**	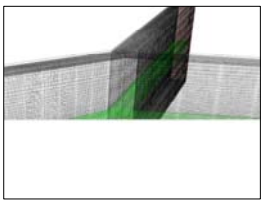	1.920.000
700	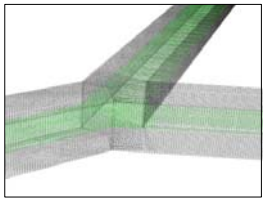	912.000	**4900**	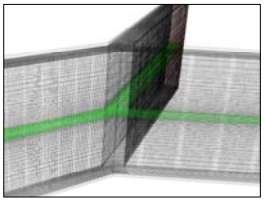	2.160.000
1400	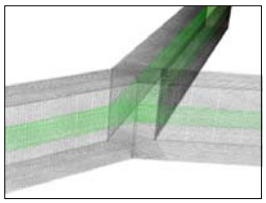	1.200.000	**5600**	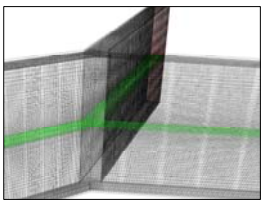	2.400.000
2100	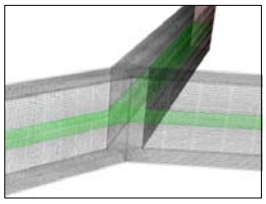	1.200.000	**6300**	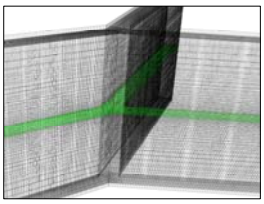	2.640.000
2800	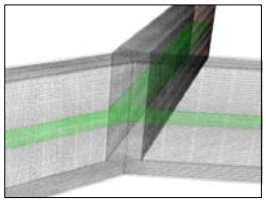	1.440.000	**7000**	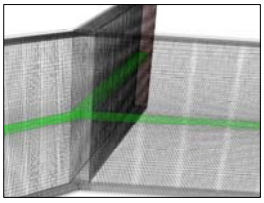	2.880.000

Reynolds number (Re) is the relevant dimensionless variable that characterizes the flow behavior of a Newtonian fluid. Control volume analysis of fully developed flow in microchannel leads to the concept of a hydraulic radius described in terms of the flow area (A) and wetted perimeter (P): $R_h = A/P$ [6].

This parameter provides a simple way of characterizing a channel of non-circular cross-section using a single characteristic length scale. In microfluidics, where is common to deal with channels of planar cross-section, it is typical to define Re as a function of the hydraulic radius $R_h = h \cdot w/2(h + w)$ and the average velocity ($V_0 = Q/h \cdot w$, where Q represents the volumetric flow rate), resulting in:

$$Re = \frac{4 \cdot \rho \cdot v_0 \cdot R_h}{\eta_0} \tag{2}$$

4. Aspect ratio influence on topological vortex structure

The analysis of all flow studies evidence three different manifestations of the vortex in the closed branch. Primarily, in geometries that present an aspect ratio $AR < 0.5$ the secondary flows are developed only at $Re \gg 100$, flow regimes that are impossible to be reproduced experimentally.

The secondary flows in the closed branch are manifested in forms of vortices. The behavior of the first vortex is manifested by its movement against the main flow. Here, the coordinates X and Y correspond to the entry of the first vortex formed in the closed branch. The different evolutions are caught in graphic representations, i.e. the Y-coordinate variation function of Re (see Fig. 1-3).

Numerical simulations performed in virtual geometries with aspect ratios of $AR = 3$ and $AR = 2$ show a non-monotonic variation on $Y(Re)$ dependence, with a minimum value localized at $Re \approx 30$ (see Fig. 1). For the geometries with high aspect ratio, $AR \geq 5$, a monoton movement of the vortex towards the main flow is observed (movement behaviour quantified in Fig. 2).

We can distinguish a major difference between the last two cases, relative to the $X(Re)$ variation: X has a monotonic increasing for $AR = 3$ and is practically constant for $AR = 10$.

For the geometry with $AR = 1$ (case from Fig. 3), the $Y(Re)$ dependence in the median plane is very similar to the geometries with $AR \geq 5$. At the same time, the movements on the X coordinate are insignificant (characteristic behavior of geometries with aspect ratios $AR > 5$). For this case, an intense study was conducted by Balan et al. [1], characterizing the dynamics of the vortex with the increasing of flow rate, with emphasis on changes induced on the local pathlines by the presence of elasticity.

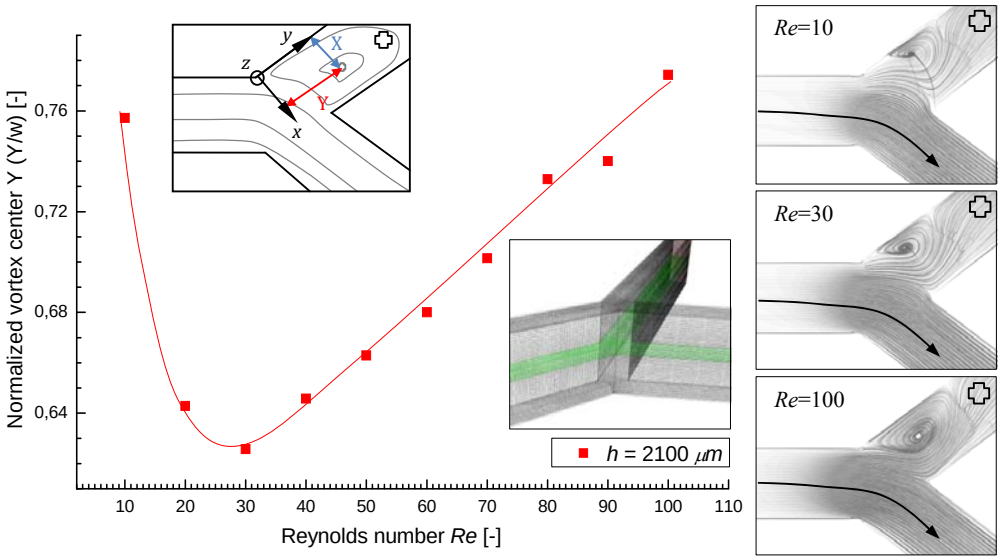

Fig. 1. Vortex evolution on Y coordinate direction for numerical predictions in case of the geometry with an aspect ratio of $AR = 3$ ($h = 2100\mu m$).

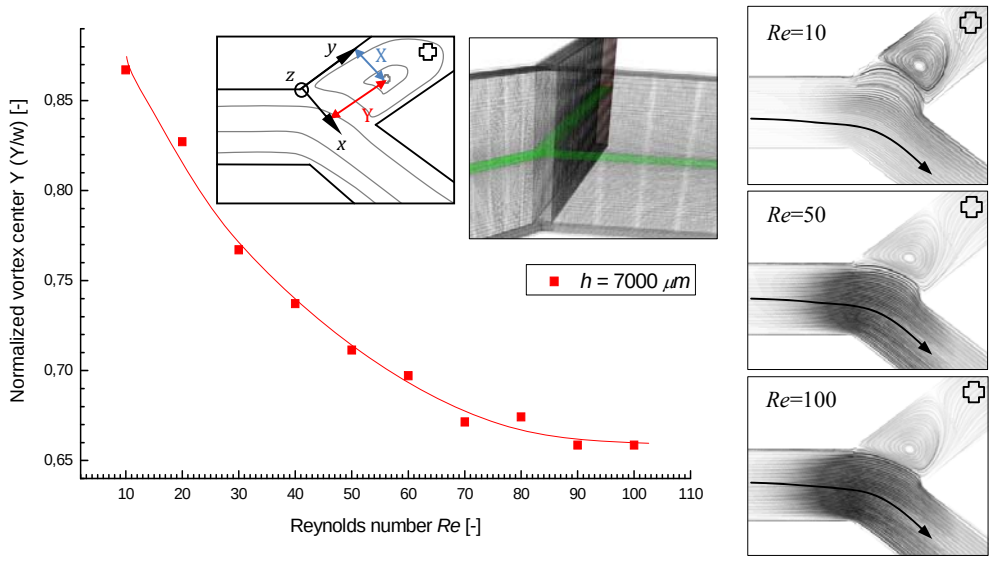

Fig. 2. Vortex evolution on Y coordinate direction for numerical predictions in case of the geometry with an aspect ratio of $AR = 10$ ($h = 7000\mu m$).

All the results for $Re < 60$(from Fig. 1, Fig. 2 and Fig. 3) show that the geometry with a square cross-sectional area can approximate quantitatively the hydrodynamics of the limiting case $AR \rightarrow \infty$ on the median plane.

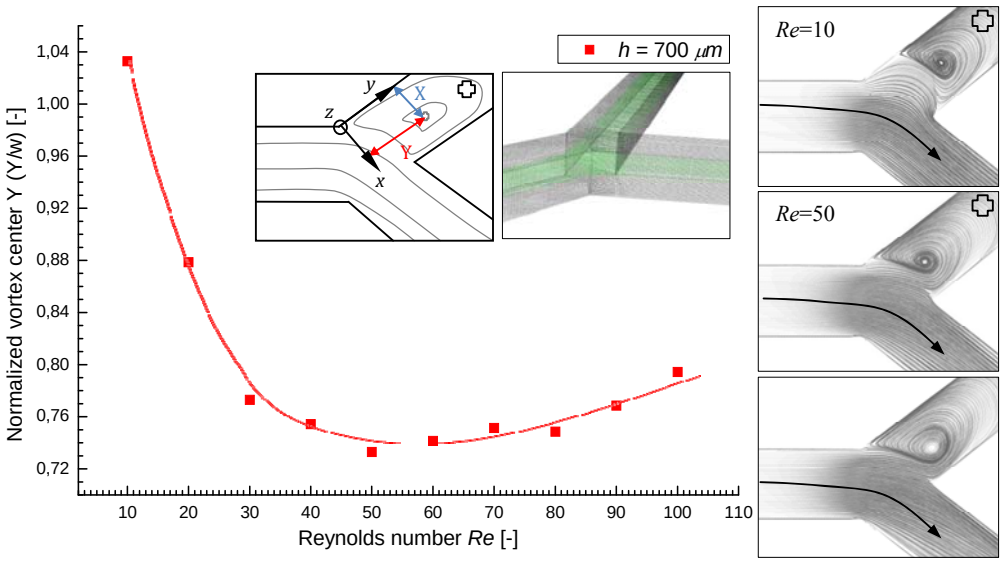

Fig. 3. Vortex evolution on coordinate direction for numerical predictions in case of the geometry ratio of $AR = 1$ (h= 7000μm).

5. Conclusions

The present numerical study was conducted for evidencing the manifestation behavior of secondary flows in Y shape microgeometries with one entry and one of the outflows maintained closed for all numerical investigations (vortex formed and developed in the closed branch of the geometry). The obtained numerical results confirm the necessity of 3D numerical simulations tested experimentally with the use of several similar geometries (in our case microbifurcations).

A detailed analysis on the secondary flows, manifested as spiraling vortical structures was made in this investigation. The graphic from Fig. 4 is quantifying the manifestation of the secondary flow - when the vortex is forming and where the vortex is moving relatively to the main flow [7]. The red symbols ( ) are evidencing the absence of secondary flows on the closed branch, the green symbols ( ) evidence the presence of the vortex and a movement of this towards the main flow, and the blue symbols ( ) are evidencing the presence of secondary flows but with a movement away of the main flow.

The developed CFD analysis can be used for a future investigation with a quantification of the boundary conditions imposed on the numerical domain, and for a validation in which a 2D numerical investigation can be conducted.

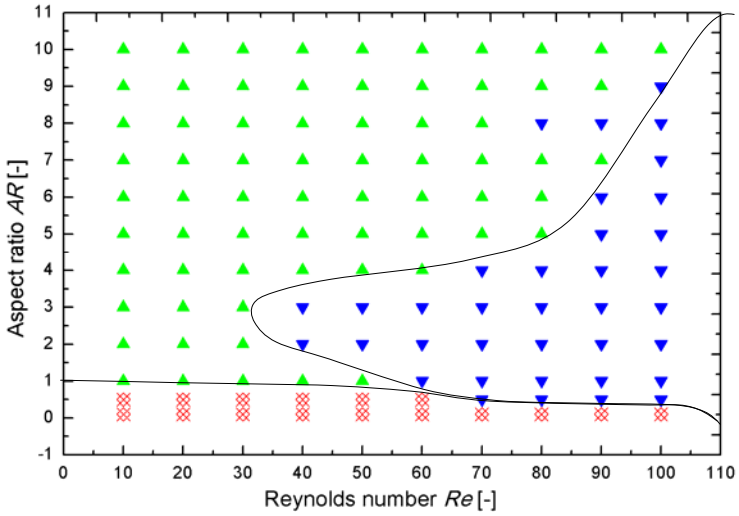

- *no secondary flows*
- *-appearance of secondary flows with a monotone movement of the vortex towards the main flow*
- *- appearance of secondary flows with a monotone movement of the vortex away of the main flow*

Fig. 4. Graphical quantification on the vortex topology evolution in different geometrical configurations (defined by different aspect ratio – AR), function of Reynolds number (Re).

6. Future work

Present numerical and experimental results will be continued with the study of vortex rings in microchannels.

The studied microgeometry consists in 3 inlets out of which: (i) the inlet for fluid 1 (dimethyl carbinol), (ii) two inlets for fluid 2 (water) and (iii) one outlet (Fig. 5).

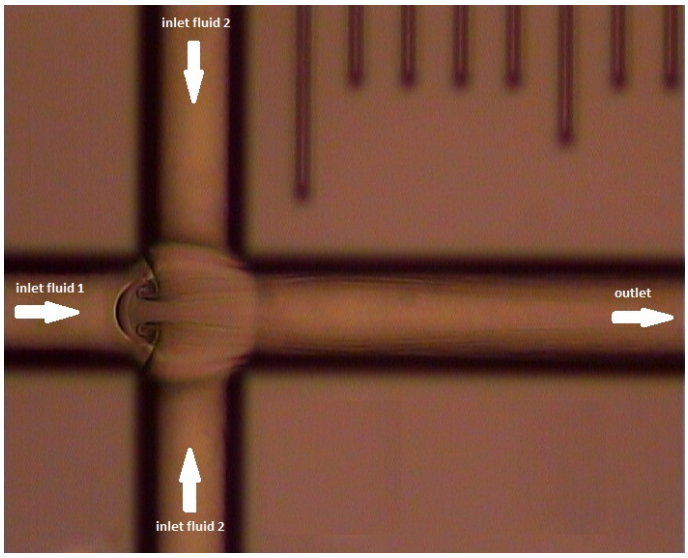

Fig. 5 Vortex ring formation in a cross microchannel with square section 100x100 μm

We observed a symmetrical structure at the interface between dimethyl carbinol and water, called vortex ring. It consists in an outer-flow and a core-fluid [8], with well-defined boundaries.

The main purpose of the future work is to perform numerical and experimental investigations of the AR influence on the vortex ring formation, as function of the input parameters.

Acknowledgement

This work was supported by grant of the Ministry of National Education, CNCS – UEFISCDI, project number PN-II-ID-PCE-2012-4-0245; Iulia-Rodica Damian and Ioana Laura Omocea acknowledge the financial support of the doctoral project InnoRESEARCH-POSDRU 159/1.5/S/132395

REFERENCES

[1]. *C. M. Bălan, D. Broboană, C. Bălan,* "Investigation of vortex formation in microbifurcations" in Journal of Microfluidic Nanofluidic, **vol. 13**, no. 5, November 2012, pp. 819-833.

[2]. *H. Bruus,* "Theoretical Microfluidics", Lectures notes second edition, fall 2005.

[3]. *Whitesides, G. M., Stroock A. D.* "Flexible methods for microfluidics" in Physics Today, v**ol**. **54**, no. 2, June 2001, pp. 42-48.

[4]. *G. Karniadakis, A. Beskok, N. R. Aluru* "Microflows and nanoflows: fundamentals and simulation". Springer Verlag, New York, 2005.

[5]. *M. S. N. Oliveira, M. A. Alves, F. T. Pinho, G. H. McKinley,* - "Viscous flow through microfabricated hyperbolic contractions" in Journal of Experiments in Fluids, **vol. 43,** no.3, May 2007, pp. 437–451.

[6]. *M. Gad-el-Hak,* "The MEMS handbook". CRC Press, Boca Raton, 2002.
[7]. *Cătălin Mihai Bălan,* "Modeling and Control of Viscous and Viscoelastic Fluids Flows in Microchannels", PhD Thesis, University Politehnica Bucharest, 2011.
[8]. *T. Maxworthy*, "Some experimental studies of vortex rings" in Journal of Fluid Mechanics, **vol. 81**, part. 3, 1977, pp. 465 - 495.